NJC

New Journal of Chemistry

A journal for new directions in chemistry

Accepted Manuscript

This article can be cited before page numbers have been issued, to do this please use: L. Miturova, I. Rodriguez-Donis and P. De Caro, *New J. Chem.*, 2026, DOI: 10.1039/D5NJ03530A.

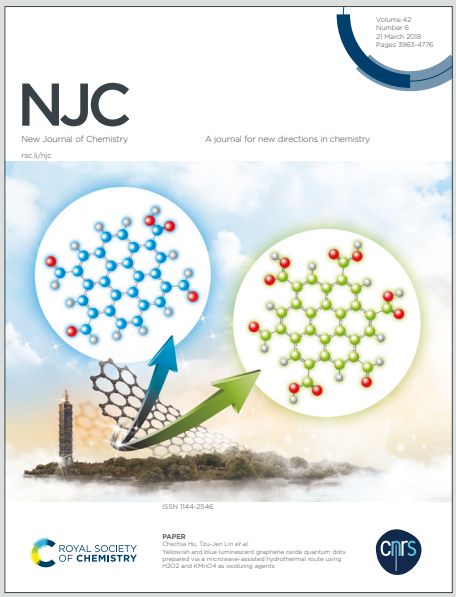

This is an Accepted Manuscript, which has been through the Royal Society of Chemistry peer review process and has been accepted for publication.

Accepted Manuscripts are published online shortly after acceptance, before technical editing, formatting and proof reading. Using this free service, authors can make their results available to the community, in citable form, before we publish the edited article. We will replace this Accepted Manuscript with the edited and formatted Advance Article as soon as it is available.

You can find more information about Accepted Manuscripts in the Information for Authors.

Please note that technical editing may introduce minor changes to the text and/or graphics, which may alter content. The journal's standard Terms & Conditions and the Ethical guidelines still apply. In no event shall the Royal Society of Chemistry be held responsible for any errors or omissions in this Accepted Manuscript or any consequences arising from the use of any information it contains.

ROYAL SOCIETY OF CHEMISTRY

rsc.li/njc

View Article Online
DOI: 10.1039/D5NJ03530A

ARTICLE

Green synthesis of glycerol carbonate using efficient mixed oxide catalysts

Linda Miturova,[a] Ivonne Rodriguez-Donis [a] and Pascale De Caro [*a]

Received 00th January 20xx,
Accepted 00th January 20xx

DOI: 10.1039/x0xx00000x

The transcarbonation reaction of glycerol (Gly) with diethyl carbonate (DEC) was investigated to synthetise glycerol carbonate (GC) using two major types of basic catalysts: conventional carbonates (K_2CO_3 and Na_2CO_3) and, for the first time in this context, metal oxides (CaO, MgO, MgO/CaO and KNO_3/CaO) calcined at 700 or 900 °C. The introduction of metal oxides as catalysts represents a novel approach for this type of transcarbonation reaction. Analyses showed that the mixed CaO based metal oxides have a porous structure suitable for the transcarbonatation reaction and higher BET surface areas compared to single CaO oxide. Two different loadings of each catalyst (5 and 10% mass related to Gly) were used with 2:1 molar excess of DEC to produce GC during 3 hours at 110 °C under mechanical stirring (500 rpm). The results showed the interest of using mixed oxides (MgO/CaO or KNO_3/CaO) calcined at the appropriate temperature, to obtain GC yields and selectivity higher than 90% without byproducts formation.

1. Introduction

Faced with increasing global demands for cleaner energy sources, biodiesel is still considered a useful biofuel when blended with the commercial diesel fuel. The usual way to produce the biodiesel is *via* the transesterification reaction of animal or vegetable oils with an alcohol, to obtain the fatty acid methyl esters (FAMEs). Glycerol as a main co-product represents 10% of the biodiesel production (1,2). Its valorisation is crucial to ensure the competitiveness of the production chain. So, glycerol is an available polyol with interesting properties for numerous industrial fields such as pharmaceutical and food industry. It is also a platform molecule for the chemical industry, to prepare new valuable chemicals (3,4).

Glycerol carbonate (4-hydroxymethyl-1,3-dioxolan-2-one) is one of the most significant derivatives of glycerol. Glycerol carbonate (GC) is a non-toxic, biodegradable molecule, stable over a wide range of temperatures, with a boiling point of 353 °C at atmospheric pressure and a melting point at -69 °C. It is considered an attractive substitute for various synthetic derivatives for many applications. For instance, GC is commonly used as an alternative solvent for nail polish remover and for gas separation membranes, as a humectant for pharmaceuticals or as a plasticizer (4,5). Currently, GC is showing greater interest as an electrolytic component of lithium batteries (6). In comparison with other carbonate-based solvents, GC has a high dielectric constant (4,7) and the ability to form a solid layer of oligomer on the interface between electrode and electrolyte, thus generating a passivation effect and enhancing the lifetime of the lithium cell (4,8). The ambivalent character of glycerol carbonate, due to the primary hydroxyl group and the 2-oxo-1,3-oxolane group (ODO), confers a large chemical reactivity to the molecule (4,8). Indeed, it is an intermediate for the synthesis of esters (9,10), biobased polyhydroxyurethanes (11), polyglycerols (12) and poly(glycerol carbonates) (12).

Various methods for the synthesis of GC from glycerol have been investigated. Direct carbonation of glycerol using phosgene present disadvantages in terms of safety and the environment (4,13). The two steps production of GC can be conducted using ethylene oxide reacting directly with CO_2 and glycerol to form GC. This route displays some thermodynamics limitations as well as the employment of a toxic ether revealing security constraints (14). Today, the reaction of glycerol with urea is one of the most studied routes of synthesis. However, this reaction goes along with high reaction temperatures (15,16) and the formation of biuret and isocyanic acid, both toxic. Furthermore, the most common catalysts are organometallic sulphates (17), prepared with sulphur dioxide considered toxic to aquatic environments (18).

Finally, the possibility to obtain the glycerol carbonate from glycerol via a transesterification reaction with a carbonate source offers good prospects. Dimethyl carbonate (DMC) has been commonly used as a source of carbonate combined with homogeneous or heterogenous catalysts for selective transcarbonation (19–23). Under these conditions, the transcarbonation reaction of glycerol to produce GC leads to a co-product, methanol, which forms an azeotropic mixture with DMC, making its separation difficult and costly (24–26). Therefore, the objective of the present work is to investigate the use

[a] *Laboratoire de Chimie Agro-Industrielle, LCA, Toulouse INP, Université de Toulouse, France*

† Electronic supplementary information (ESI) available: ESI containing detailed corrected results of catalyst screening and example of mass balance calculations. See DOI: 10.1039/x0xx00000x

View Article Online DOI: 10.1039/D5NJ05730A

of diethyl carbonate (DEC) to replace the DMC as carbonate source. This alternative pathway generates ethanol as a co-product without forming an azeotropic mixture with the reactant DEC (27). The scheme of the reaction is presented on Figure 1. The transcarbonation reaction involves two successive nucleophilic attacks of the primary and secondary hydroxyl groups of glycerol on dialkyl carbonate, leading to the departure of the corresponding alkoxide ion. With diethyl carbonate, ethanoate ions are released, but methanoate is a better leaving group compared to ethanoate (28), as the latter is destabilized by the higher electron density on its partially negatively charged oxygen atom. The removal of high purity ethanol during the reaction is possible, as it is the most volatile components of the system, which also helps shift the equilibrium towards the formation of the desired product. The employment of a DMC substitute for the transcarbonation reaction of glycerol was rarely reported in the literature and was typically associated with the use of complex catalysts containing rare metals. For example, studies using Mg/Al based catalysts (hydrotalcite-like compounds) have been reported, although they require long reaction times, reaching only 76% yield after 50 hours of reaction at 130 °C (29) or 80% of glycerol conversion after 8 hours at 130 °C (30). Souza Junior et al. (2023) tested Ca/Al based catalyst in the presence of DMSO, achieving a 91% yield of glycerol carbonate after 5 hours at 130 °C (31). CeO_2 based catalysts mixed with Ni oxide were used by Wu et al. (2017), for the synthesis of CG from DEC, with 94% glycerol conversion and GC selectivity of 90.95% after 8 hours at 85 °C (32). Andola et al. (2025) have recently synthetised GC from glycerol and DEC by adding 20% of $NaAlO_2$ catalyst prepared by spray drying and sonication methods, using glycerol-F127 template to increase its surface area. In their work, a large excess of DEC was used (1:4 molar, Gly:DEC) at 90 °C, to obtain 92% of Gly conversion and 100% of GC selectivity after 3 hours , using the complex $NaAlO_2$ catalyst system (33).

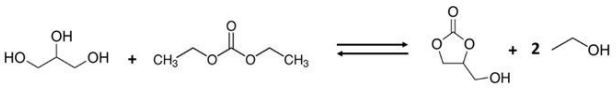

Figure 1: Transcarbonation reaction of glycerol and DEC to produce GC and ethanol

So, the present study involves the screening of readily available catalysts, such as oxides and carbonates of alkaline earth and alkali metals, to develop efficient conditions for the production of glycerol carbonate (GC) *via* the transcarbonation reaction of glycerol and diethyl carbonate (DEC) in 3 hours at 110 °C. The performances of catalysts are compared in terms of glycerol conversion, GC yield, and selectivity. To our knowledge, such catalysts have never been studied for this chemical route. Some of these catalysts have already been tested for the transesterification reaction of glycerol with DMC **(3,34)**. The choice of the catalyst focuses on three main criteria: high activity, chemical stability and cost. We selected two earth metal carbonates (K_2CO_3 and Na_2CO_3), two metal oxides (CaO and MgO), and mixed metal oxides based on active calcium oxide core (MgO/CaO and CaO mixed with potassium cations using KNO_3/CaO catalyst). The study also aims to understand which characteristics of these catalytic systems are crucial to improve the performances of the transcarbonation reaction when replacing DMC by DEC. Therefore, the preparation of the heterogeneous catalysts and their characterisation are preliminary steps.

2. Experimental Methods

2.1 Materials and chemicals

Anhydrous glycerol (high purity of ≥ 99%) was supplied by Reagent Plus, Sigma (USA). Anhydrous diethyl carbonate (DEC) of purity 99% was obtained from Thermo Fisher Scientific (USA). HPLC isocratic grade absolute anhydrous ethanol was obtained from CARLO ERBA Reagents (Italy). The catalysts, K_2CO_3 ACS reagent, ≥ 99.0% and Na_2CO_3 99%, were supplied by Sigma (USA). The metal oxides MgO 95% and CaO, reagent grade, were obtained from Sigma (USA). No further treatments were applied on the reagents mentioned previously.

Standard quality glycerol carbonate (GC) was supplied by Huntsman (USA) and purified using a thin film evaporation to obtain the final purity of 95-98%. Ion exchange resin amberlite 120H R was supplied by Sigma (USA). HCl, 36% used to regenerate the resin was obtained from Thermo Fisher Scientific (USA).

2.2 Preparation of simple and mixed oxide catalysts

2.2.1 Preparation of homogeneous catalysts

Sodium carbonate and potassium carbonate were both dried at 105 °C under static air for at least 4 hours before the experiments. They were both stored in a desiccator under reduced controlled humidity, maintained between 20 to 29% depending on the temperature, which varied from 16 to 27 °C.

2.2.2 Preparation of simple and mixed heterogeneous catalysts

Magnesium and calcium oxide were calcined in the air furnace at 800 °C during 3 hours before using them for the reaction. For the preparation of mixed oxide MgO/CaO, individual metal oxides were previously calcined at 550 °C for 12 hours, followed by sieving through 1 mm mesh. Then the mixed metal oxide catalyst was prepared by mechanical mixing of MgO and CaO, with the mass ratio of metal ions Ca^{2+}: Mg^{2+} of 1:1.1, according to the adapted protocol of Khayoon and Hameed (2013) (3). The mixture was calcined at 800 °C, then sieved through 500 µm mesh and stored in a desiccator.

The mixed metal oxide catalyst KNO_3/CaO was prepared by dry impregnation. First, CaO was dried at 105 °C during 4 hours, then calcined in air furnace at 550 °C for 12 hours to remove the physiosorbed water and activate the catalyst. Then, it was mixed with an aqueous solution of KNO_3 prepared as follows: 2.15 g of KNO_3 were dissolved in 25 mL of distilled water, according to the protocol of Hu and al. (2015) (34). The solution was homogenised by the

ultrasound and stirred at room temperature for 10 min. Then 10 g of the calcined CaO powder were added, the mixture was stirred for 15 min and set to equilibrate for 48 hours at ambient temperature. Subsequently, the mixture was dried at 105 °C for 24 hours and calcined under static air at 700 °C for 5 hours (KNO_3/CaO 700) and 900 °C for 3 hours (KNO_3/CaO 900), using the heating ramp of 2.5 °C/min. The prepared mixed catalysts were sieved at 500 µm mesh and stored in desiccator. Before their use, the catalysts were dried at 105 °C for 4 hours, to remove the possible remaining physisorbed water.

2.3. Catalyst characterisation

2.3.1. Inductively coupled Plasma - Atomic Emission Spectroscopy (ICP-AES)

The samples were analysed using iCAP 6300 thermo generator RF equipped with a CID optical detector (LCC, Toulouse, France). The mineralization was performed using a mixture of HNO_3 and HCl (1:3 v/v) for 1 hour. Mg, Ca and K contents were determined.

2.3.2. X-ray diffraction

X-ray diffraction patterns of simple or mixed metal oxide catalysts were recorded on a Rigaku Miniflex 600 powder diffractometer in the θ/2θ configuration, equipped with a Cu anode X-ray tube and a HyPix 400 MF 2D hybrid pixel detector. The diffractograms were processed using the Panalytical Highscore+ software. Results were compared with data from the Crystallography Open Database (COD).

2.3.3. Fourier Transform Infrared Spectroscopy

The Fourier Transform Infrared Spectroscopy FT-IR Spectrometer: Perkin Elmer Spectrum 65 (Walthan, MA, USA) was used at room temperature over a frequency range of 4000 to 400 cm^{-1} with a resolution of 4 cm^{-1} and 64 scans. KBr pellets (300 mg, dried at 105 °C for 12 hours and stored in a desiccator) were used as the support medium for analyses.

2.3.4. Scanning Electron Microscopy (SEM)

The surface morphology of metal oxide catalysts was studied with a Quanta 450 Scanning Electron Microscope (Hillsboro, OR, USA) operating at 5 and 15 kV, under a partial water pression of the chamber of 130 Pa with high vacuum mode.

2.3.5. Brunauer-Emmett-Teller (BET) surface analysis

The total surface area, pore volume, and average pore diameter of the catalyst were studied through an N_2 physisorption analyser, a TriStar II device from (Micromeritics, USA). Nitrogen adsorption/desorption isotherms were measured at -195.8 °C (CIRIMAT, Toulouse University). Prior to analysis, catalyst samples were degassed with N_2 at 100 °C for 3 hours. BET method was used to determine the specific surface area of catalysts at the relative pressure (p/p_0) range of 0 to 1. Barrett-Joyner-Haleda (BJH) method was used to calculate the pore size distribution, from the adsorption isotherms.

2.3.6. Thermogravimetric analysis (TGA)

The thermal stability of metal oxides was studied using Mettler Toledo TGA 2 (Mettler Toledo, Greifensee, Switzerland) under nitrogen atmosphere from 25 to 1100 °C with a heating rate of 5 °C/min, followed by an isotherm at 1100 °C for 10 min.

The thermal decomposition study of pure KNO_3 was carried out on Mettler Toledo TGA/DSC 3+ Thermal Analysis system (Mettler Toledo, Greifensee, Switzerland) by mimicking the conditions used during the calcination of the KNO_3 900 catalyst under nitrogen atmosphere from 25 to 900 °C with a heating rate of 5 °C/min, followed by an isotherm at the maximum temperature for 3 hours.

2.3.7 Basic strength evaluation by the Hammett indicator method

The basicity of the catalyst was determined using the Hammett indicator method, adapted from the procedure reported by Hu et al. (2015) (34). The basic strength of each catalyst was characterised on the Hammett scale using a series of colour indicators: phenolphthalein (H_- = 9.3), 2,4-dinitroanilline (H_- = 15.0), 4-nitroaniline (H_- = 18.4) and aniline (H_- = 27.0). Prior to the basicity measurements, each catalyst sample was dried at 105 °C for 3 hours. Subsequently, 1 g of the dried catalyst was dispersed in pure cyclohexane, and a few drops of the indicator solution (0.5 wt.% Hammett indicator dissolved in toluene) were added to the suspension. After 2 hours of contact, the colour changed of the mixtures was observed visually to determine the corresponding basicity.

2.4. Catalytic reaction

The transcarbonation reaction was conducted in a 250 mL batch reactor equipped with a double jacket, connected to a silicone oil thermostatic bath, was used to maintain a constant reaction temperature. In the reactor, 10 g of glycerol were mixed with 25.66 g of DEC, corresponding to a Gly: DEC molar ratio of 2:1. Either 0.5 or 1.00 g of catalyst (5 and 10 wt% relative to glycerol) was added. The mixture was then heated at 110 °C and stirred mechanically at 500 rpm for 3 hours. Two experimental trials were conducted for each catalyst to verify the repeatability of the results. After the completion of reaction, the reactional medium was cooled and the catalyst was separated either through cationic filtration resin for the compounds displaying homogenous behaviour, or by centrifugation (5 min, 20 °C, 3800 g force) for the heterogeneous catalysts. Finally, the distillation under reduced pressure was used to evaporate the most volatile compounds (formed EtOH and remaining DEC) contained in the filtrate and supernatant.

2.5. Product analysis

The final product was analysed by Gas Chromatography (GC-FID) with an automatised injection workstation (Varian 3900), equipped with a CP-WAX 52 CB WCOT fused silica column and a flame ionization detector (GC-FID). Samples were diluted in ethanol with dilution factor ranging from 20 to 180 in order to respect the maximum saturation concentration. The tetra(ethylene glycol) (TEG) was used as the internal standard. The carrier gas used was helium at 1.2 mL/min. The injector split ratio was 80 and the temperature

View Article Online DOI: 10.1039/D5NJ05730A

was 220 °C. The oven temperature was initially set at 60 °C (1 min) followed by ramping of 20 °C/min to 240 °C and hold for 5 min. The FID temperature was maintained at 250 °C.

The following equations, equations 1-3, were used to calculate glycerol conversion (Conversion Gly), glycerol carbonate yield (Yield GC) and glycerol carbonate selectivity (Selectivity GC).

$$Conversion\ Gly\ (\%) = \frac{moles\ of\ Gly_{\ initial} - moles\ of\ Gly_{unreacted}}{moles\ of\ Gly_{initial}} \times 100 \quad (1)$$

$$Yield\ GC\ (\%) = \frac{moles\ of\ GC_{\ produced}}{moles\ of\ Gly_{initial}} \times 100 \quad (2)$$

$$Selectivity\ GC\ (\%) = \frac{moles\ of\ GC_{\ produced}}{moles\ of\ Gly_{\ initial} - moles\ of\ Gly_{unreacted}} \times 100 \quad (3)$$

3. Results and discussion

3.1. Catalyst characterisation

3.1.1. Inductively coupled Plasma – Atomic Emission Spectroscopy (ICP- AES)

Table 1 and Table 2 show the compositions of three catalysts determined by ICP-AES.

Table 1: Elementary composition of MgO-CaO mixed catalyst

	Mg (wt. %)	Ca (wt. %)	R (Mg/Ca)	R calculated (Mg/Ca)
MgO/CaO	37.5	24.15	1.55	1.2

Table 2: Elementary composition of K-CaO 700 and 900 catalysts

	K (wt. %)	Ca (wt. %)	R (K/Ca)	R calculated (K/Ca)
KNO_3/CaO 700	2.77	47.16	0.058	0.12
KNO_3/CaO 900	1.10	63.84	0.017	0.12

For the mixed MgO/CaO catalyst, the atomic mass ratio R observed experimentally (*Table 1*) is higher than the initial mass ratio used to prepare the catalyst (R (Mg/Ca) initial = 1.1). This discrepancy may be due to the heterogeneous distribution of various atoms within the sample as described by Koranian (2024) for the same types of oxide (35). In the case of the mixed metal oxide KNO_3/CaO, the analysed atomic mass ratio R (K/Ca) (*Table 2*) is lower than the one used initially (R (K/Ca) initial = 0.12). Additionally, ICP-AES analyses reveal that the catalyst calcined at 700 °C has a higher percentage of potassium atoms and lower abundance of calcium atoms than its counterpart calcined at 900 °C. The calcination temperature is then likely to influence the atomic composition of the minerals. Freeman (1956) reported that potassium nitrate decomposes in the presence of oxygen at elevated temperatures. Above 650 °C, potassium nitrate is converted into potassium nitrite, which subsequently undergoes complete decomposition at around 790 °C (36). It has been proposed that the potassium atoms released during this process react directly with atmospheric oxygen, leading to the formation of potassium oxides outside the crystalline lattice (37). The thermogravimetric analysis was carried out on pure KNO_3 (Figure 1 of ESI †). The mass loss of 73% was observed at around 760 °C, therefore confirming these assumptions. As a result, the potassium content decreases progressively with increasing temperature. In contrast, calcium oxide remains stable between 700 and 900 °C (38). These findings can also explain the variations observed between the atomic compositions measured before calcination and those determined by ICP-AES on the calcined samples.

3.1.2. Structure analysis: X-ray diffraction

Stability of MgO/CaO catalyst

The XRD pattern of Figure 2 a) shows a hexagonal (P -3 m1) crystalline pattern characteristic of Portlandite, $Ca(OH)_2$ (2θ = 18.1°, 28.7°, 34.2°, 47.3°, 50.8°, 54.5°, 56.3°, 62.8°, and 64.4°). The absence of characteristic CaO (lime) diffraction peaks (2θ = 32.2°, 37.4°, 53.9°, 64.1°, 67.4°) may be attributed the sample's exposure to ambient humidity during analysis. The diffractogram obtained for the calcined MgO sample (Figure 2 b)) confirms the presence of the cubic crystalline phase (F m -3 m), Periclase with characteristic peaks at 2θ = 36.9°, 42.9°, 62.3°. The calcined mixed oxide MgO/CaO exhibits three different patterns: cubic CaO, hexagonal $Ca(OH)_2$ and cubic MgO (Figure 2 c)). Unlike simple CaO sample, the mixed metal oxide MgO/CaO exhibits the presence of the cubic CaO form. This result confirmed the influence of MgO, particularly Mg^{2+} ions, in the restructuring of the crystal lattice. Indeed, the presence of cubic MgO is supposed to protect the active Ca^{2+} species (39,40).

The advantage of mixed MgO/CaO catalyst is to avoid the degradation of calcium oxide into hydroxide/carbonate according to the mechanisms described by equations 5 and 6 (41,42):

$$CaCO_{3\,(s)} \leftrightarrow CaO_{(s)} + CO_{2\,(g)} \quad (5)$$

$$Ca(OH)_{2\,(s)} \leftrightarrow CaO_{(s)} + H_2O \quad (6)$$

The catalyst becomes then less sensitive to contact with air (interaction with humidity and CO_2), thus preserving its initial active form.

Effect of calcination temperature on the crystal structure of KNO_3/CaO catalyst

The mixed oxides, KNO_3/CaO 700 and 900 (Figure 2 d) et e)), mainly exhibit a crystal pattern corresponding to Portlandite ($Ca(OH)_2$). For the KNO_3/CaO sample calcined at 700°C, the peak at 2θ = 37.4° can be attributed to cubic calcium oxide pattern and the one at

View Article Online
DOI: 10.1039/D5NJ03530A

2θ = 29.5° corresponds to the orthorhombic structure of KNO_3 according to Hu and al. (34) . The decomposition of potassium nitrate is believed to begin at 650 °C (43) following the mechanisms outlined below in equations 7 - 9. For the mixed oxide calcined at 900 °C, the cubic CaO and orthorhombic KNO_3 patterns are absent, as shown in equations 8' and 9'. It can be assumed that KNO_3 reacted with CO_2 and H_2O (air), thus rearranging the crystal structure to form potassium oxide (K_2O, a highly reactive compound) and potassium hydroxide (KOH, a stable molecule).

$$KNO_3 \rightarrow KNO_2 + {}^1/_2\, 0_2 \quad (7)$$

$$2KNO_2 \rightarrow K_2O + NO_2 + N_2 \quad (8)$$

followed by $K_2O + H_2O \rightarrow KOH$ (8')

$$2KNO_2 \rightarrow K_2O + N_2 + {}^3/_2\, O_2 \quad (9)$$

followed by $K_2O + CO_2 \rightarrow KOH$ (9')

K_2O and KOH can accumulate inside the pores of CaO, resulting in a reduction of the active surface area of the catalyst (35,44).

This phenomenon could be responsible for the restructuring of KNO_3/CaO network calcined at 900 °C, thus decreasing its catalytic activity compared to its analogue calcined at 700 °C.

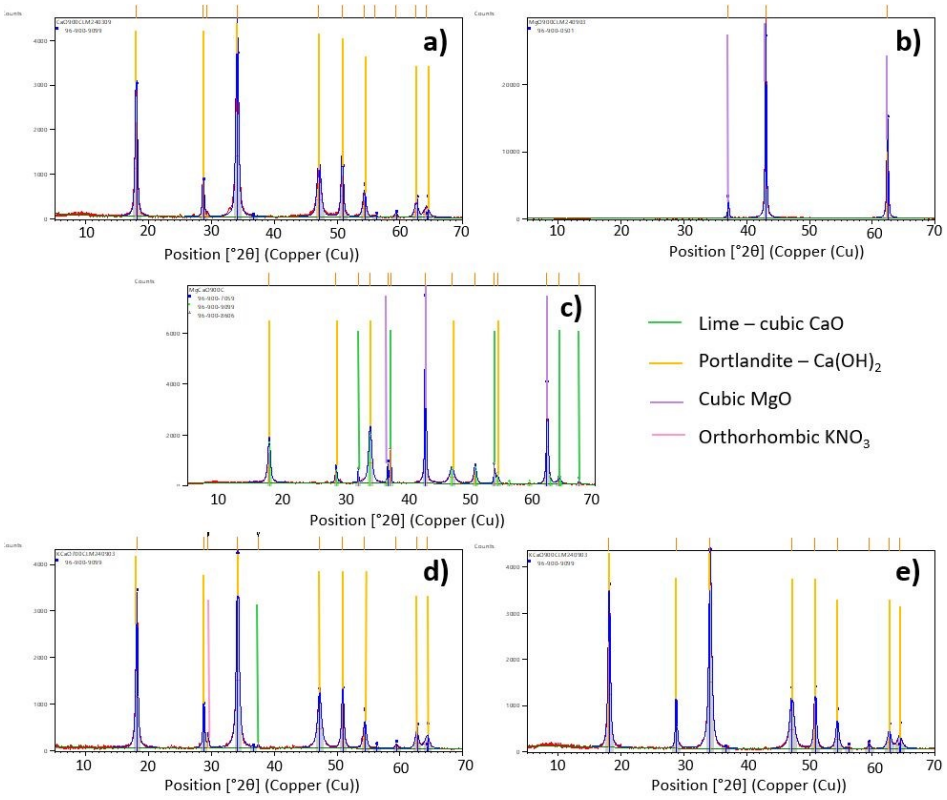

Figure 2: XRD pattern for calcined catalysts: a) CaO; b) MgO; c) MgO/CaO; d) KNO_3/CaO 700; e) KNO_3/CaO 900

3.1.3. Fourier Transform Infrared Spectroscopy

The Fourier Transform Infrared Spectroscopy was used to identify the characteristic functions of catalyst samples.

Characterization of homogeneous catalysts

For K_2CO_3 and Na_2CO_3, two strong bands were observed in Figure 3, at 1647 cm^{-1}, 1400 cm^{-3} (K_2CO_3) and 1439 cm^{-1} (Na_2CO_3). These bands are attributed to the typical asymmetric stretching of C-O bond. The C-O stretching at 1400 cm^{-1} is usually allocated to aliphatic carbonate function. However, the C-O band at 1647 cm^{-1} is more likely to be assigned to the presence of the bicarbonate group. The same observation was made by Alonso and al. (2007) when studying the K_2CO_3/γ Al_2O_3 mixed catalyst (45). Bicarbonates are formed from carbonates in the presence of water (air) and CO_2 (air) due to the deprotonation of carbonic acid according to equations 10 and 11. The band at 850 cm^{-1}, corresponding to the bending of the O-C=O group (carboxylate ion) (44), appears in the spectra of both compounds, as shown in Figure 3. The O-H bond vibrations observed between 3700 and 3000 cm^{-1}, indicate traces of physisorbed water.

$$Na_2CO_3 + H_2O + CO_2 \leftrightarrow 2NaHCO_3 \quad (10)$$

View Article Online
DOI: 10.1039/D5NJ03530A

$$K_2CO_3 + H_2O + CO_2 \leftrightarrow 2KHCO_3 \text{ (11)}$$

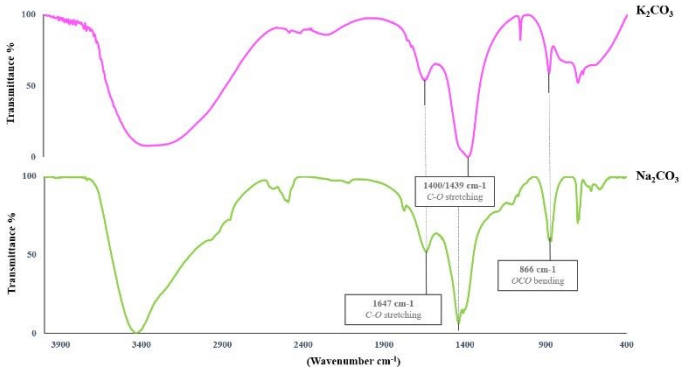

Figure 3: FT-IR Characterisation of dried homogeneous catalysts

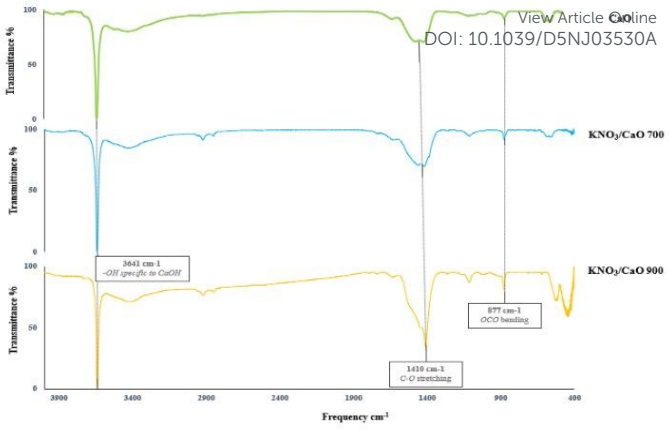

Figure 5: FT-IR characterisation of calcined heterogeneous catalysts - CaO, KNO_3/CaO 700, KNO_3/CaO 900

Characterization of heterogeneous catalysts

The infrared spectra of calcinated metal oxides (MgO and CaO) and mixed oxides (MgO/CaO and KNO_3/CaO 700 and 900) are shown in Figure 4 and Figure 5. For calcium oxide and mixed catalyst samples, a strong band at 3640 cm^{-1} was observed, which can be attributed to the OH group specific to $Ca(OH)_2$. The formation of the hydroxide species occurs when the oxide interacts with water molecules. For the heterogeneous catalysts studied, the signal in the region between 1480 and 1400 cm^{-1} corresponds to the C-O stretching of CO_3^{2-} ions (44), as observed for homogeneous catalysts. A slight bending band of the OCO group appears at 875 cm^{-1} (44) for CaO, MgO/CaO, KNO_3/CaO 700 and KNO_3/CaO 900. In Figure 4, MgO displays a band at 635 cm^{-1}, corresponding to a cubic form, as described by Wang and al. (46). This vibration is also observed in the mixed oxide MgO/CaO sample. In Figure 5, the absence of a nitrate ion stretching band around 825 cm^{-1} for the mixed KNO_3/CaO catalysts, indicates that the impregnation was complete as described by Olutoye (47).

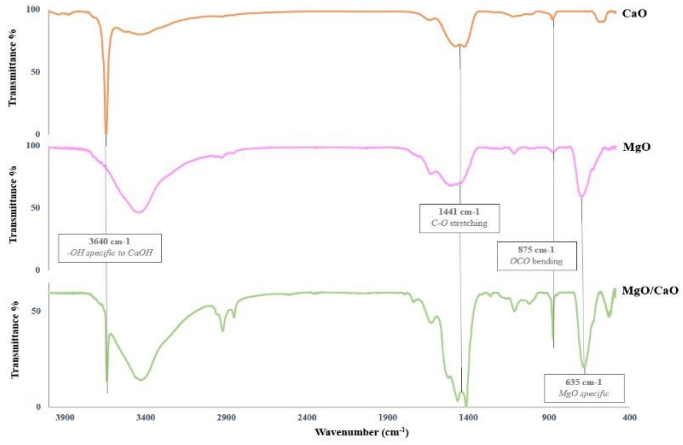

Figure 4 :FT-IR characterisation of calcined heterogeneous catalysts - CaO, MgO, MgO/CaO

3.1.4. Scanning Electron Microscopy (SEM)

The surface morphology of the different catalysts was analysed by SEM. First, the magnification of the two simple metal oxide catalysts CaO and MgO (Figure 6), showed heterogeneously sized dispersion crystalline aggregates. Figure 7 shows CaO particles consisting of stacked crystalline microstructures in the form of smooth cuboids ranging in size from 4 to 16 µm. Metallic oxides often exhibit cuboidal clusters (3) while images of a pure MgO sample (Figure 6 (b) et Figure 8 (c)) show spherical structures with rough surface.

The formation of "bird's nest" shaped like crystals typical of oxide form begins at 100 °C for $MgCO_3$ (48). Zhou and al. (2011) highlighted the presence of rough microspheres with rose petal-like surface artifacts, after calcination (500 °C for 3 h) of magnesium oxide (49). Thereby, as shown in Figure 8(c) at 3000X magnification, SEM analysis of MgO calcined at 800 °C shows oxide microspheres with similar structures, the spheres with rough surface (bird's nest or rose petal-covered surface as artifacts).

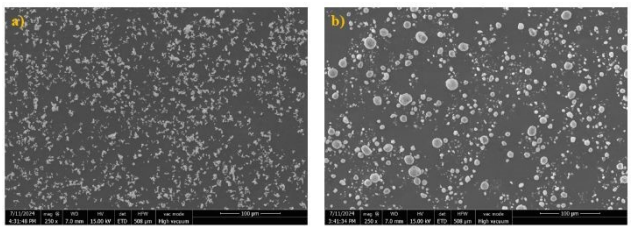

Figure 6: SEM images (magnification 250x at 15.00 kV) of CaO (a); and MgO (b)

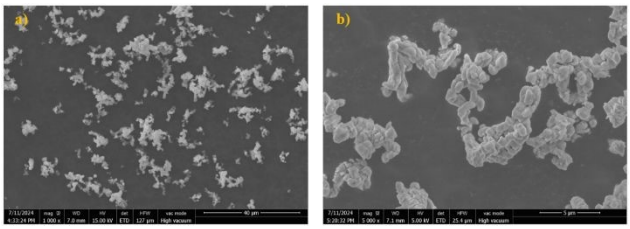

Figure 7: SEM images of CaO, (a) magnification 1000x at 15.0 kV; (b) magnification 5000x at 5.00 kV

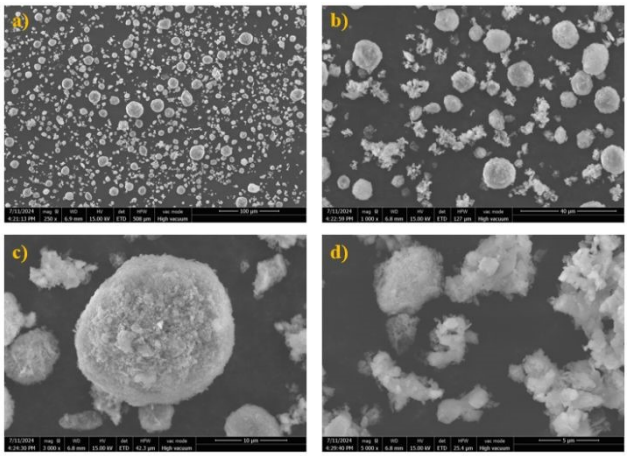

Figure 8: SEM images of MgO/CaO at 15.00 kV, (a) magnification 250x; (b) magnification 1000x; (c) zoom on MgO particles with magnification 3000x; (d) zoom on cubic structures with magnification 5000x

The MgO/CaO catalyst exhibits a heterogeneous dispersion of aggregates with two types of structures: spherical and stacked cuboid of varying sizes, ranging from 2 to 30 µm. The spherical structures are slightly larger and more abundant (Figure 8(a) and (b)). The crystalline forms of the stacked cuboids and spheres correspond to CaO and MgO, respectively. Unlike pure CaO, the CaO crystals in the mixed oxide MgO/CaO have a rough surface. This may be due to the deposition of fine MgO particles (Figure 9) as suggested by Koranian and al. (35). Furthermore, a deeper electron penetration (15 kV) showed dumbbell-shaped CaO crystals (Figure 8 (d)), a typical structure of oxides as described by Khayoon and al. (3). Other crystals are in cubic form within different crystal stacks also showing the presence of an oxide structure as confirmed by Taufiq-Yap (50).

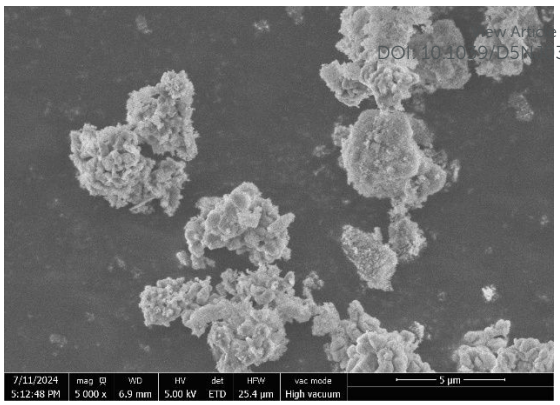

Figure 9:SEM image of MgO/CaO calcined at 800°C, zoom on CaO stacking with magnification 5000x at 5.00kV

KNO_3/CaO calcined at 700 °C exhibits structures with homogeneous morphology (Figure 10 (b)), resembling a stack of quasi-laminar sheets or oat flakes (Figure 10 (c)). In contrast, the same compound prepared at 900°C displays stacked cuboid structures with some dumbbell-shaped crystals (Figure 10 (e)). Some crystals have surface roughness and deposits of small particles of various shapes (Figure 10 (d)). KNO_3/CaO catalysts exhibit homogeneous particle dispersion with larger crystalline aggregates for the catalyst calcined at 900 °C (Figure 10 (a) and (d)). This observation indicates that the size of crystalline particles increases with calcination temperature. Indeed, Hu and al. (2012) observed that a high calcination temperature tends to aggregate oxide particles (34). In general, larger aggregates are not favourable to catalytic activity.

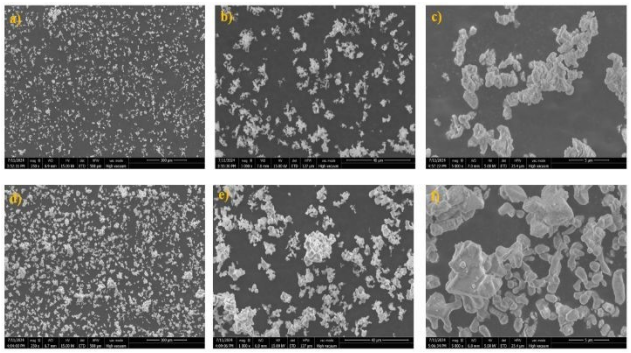

Figure 10: SEM images (magnification, electron penetration) of KNO_3/CaO calcined at 700°C; (a) 250x, 15.00kV; (b) 1000x, 15.00kV; (c) 5000x, 5kV and KNO3/CaO calcined at 900°C; (d) 250x, 15.00kV; (e) 1000x, 15.00kV; (d) 5000x, 5.00kV

3.1.5. Textural properties – BET analysis

Table 3 gathers BET analysis results for the heterogeneous catalysts.

View Article Online
DOI: 10.1039/D5NJ03530A

Table 3: BET analysis results of heterogenous catalysts

	BET surface (m^2/g)	Total pore volume (cm^3/g)	Total pore surface area (m^2/g)	Average pore diameter (nm)
CaO	6.9	0.011	4.9	40.8
MgO	20.6	0.029	22.2	37.1
MgO/CaO	15.2	0.025	17.7	36.2
KNO_3/CaO 700	7.8	0.012	6.6	31.6
KNO_3/CaO 900	3.3	0.005	2.2	36.5

Specific surface area and particle size (BET surface area)

The BET surface areas obtained for CaO and MgO calcinated at 800 °C are similar to the values found in the literature for the oxide calcinated at 850 °C, which are 2.7 m^2/g and 24.7 m^2/g, respectively (3). For the other catalysts calcined at 800 °C, the values obtained are slightly lower than those reported in the literature: 31.7 m^2/g for $Mg_{1.2}Ca_{0.8}O_2$ (3), 11.2 m^2/g for Mg-Ca mixed oxide 1:1 (35), 11.1 m^2/g for KNO_3/CaO (34), 12.6 m^2/g for KNO_3/CaO calcined at 900 °C (34). The differences between the obtained results and literature data for these samples are probably due to variations in catalyst preparation and analysis conditions. Brief exposure to moisture could cause particle agglomeration, thereby limiting access to the pores.

According to SEM analysis, the particle sizes of the KNO_3/CaO 900 sample were higher than those of KNO_3/CaO 700, (Figure 10 (a) and (d)). This suggests that particle agglomeration is promoted by the calcination temperature, which can explain the decrease in the specific surface area, as previously discussed in literature (3,34).

Porosity

The average pore diameters of the catalysts are between 30 and 45 nm (Table 3) indicating that these metal oxides are mesoporous. According to the International Union of Pure and Applied Chemistry (IUPAC), mesoporous materials have an average pore diameter between 2 and 50 nm (51).

The nitrogen adsorption-desorption isotherms are showed in Figure 2 of ESI †. The five catalysts exhibit the type IV isotherm as well as the typical point B. Such type of isotherm is linked to mesoporous materials. A slight hysteresis loop is observed for CaO (Figure 2 of ESI † (a), MgO (b), MgO/CaO (c) and KNO_3/CaO 900 (e)), indicating that these isotherms could be classified as type IVa. The isotherms of mixed oxide KNO_3/CaO 700 correspond to isotherm type IVb (Figures 2 of ESI † (c) and (d) respectively) because of the missing hysteresis loop. The absence of a hysteresis loop suggests smaller mesopores with fully reversible capillary condensation (52). This indicates the presence of interconnected pores of varying sizes which may improve the diffusion of the reagents on the catalyst surface, thus enhancing the catalytic activity (53).

3.1.6. Thermogravimetric analysis (TGA)

Error! Reference source not found. shows TAG graphs corresponding to analysis of four heterogeneous catalysts.

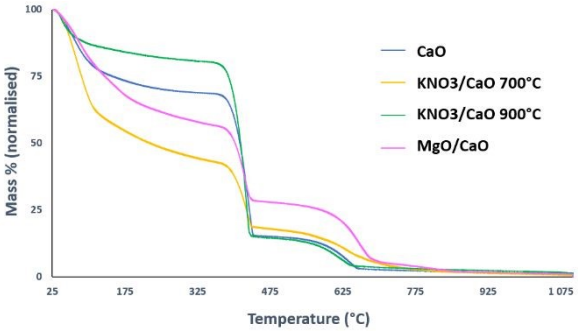

Figure 11:Thermograms of the heterogenous metal oxide catalyst

For the four analysed compounds (CaO, KNO_3/CaO 700, KNO_3/CaO 900, and MgO/CaO), three mass losses are observed. The first mass loss between 50 and 100 °C can be associated with the evaporation of undissociated water present in the samples. The loses are ranging from 3 to 43% depending on the hygroscopicity of the catalyst. For this temperature range, KNO_3/CaO calcined at 900 °C (3% mass loss) shows a lower water mass loss, compared to its counterpart calcined at 700 °C, which loses 43% of its mass. The second mass loss, (10% to 20%) taking place between 300 and 500 °C, is associated with the removal of hydroxyl functional groups. The presence of OH function results from the dissociative chemisorption of water molecules, where the first step is the formation of OH groups on the oxide surface through complexation with cations (Ca^{2+}, Mg^{2+}, K^+) (16). The final mass loss occurs between 600 and 650 °C and corresponds to the dissociation of carbonate groups formed when oxides interact with carbon dioxide from the air.

These results confirm the choice of the calcination temperature for catalysts activation to ensure their oxide form. For the four samples, an activation temperature above 650 °C should lead to only oxide forms.

3.1.7. Basic strength evaluation by the Hammett indicator method

The basic strength of the catalysts was evaluated using the Hammett indicator method. When a colour change occurs in the presence of a given indicator, the basic strength of the catalyst is considered higher than the corresponding Hammett function value (H_).

For the simple oxides, the CaO catalyst did not induce any colour change with the tested indicators, indicating a basic

strength lower than H_ = 9.3. MgO caused a colour transition of phenolphthalein from colourless to pink but did not affect 2,4-dinitroaniline, suggesting a basic strength in the range of 9.3 < H_ < 15.0. A similar behaviour was observed for the mixed KNO_3/CaO 900 catalyst, whose basicity also fell within this interval. The KNO_3/CaO 700 mixed oxide induced a colour change in 2,4-dinitroaniline (from yellow to brown) but not in 4-nitroaniline (H_ = 18.4), indicating a basic strength between 15.0 < H_ < 18.4. Among all the tested catalysts, the MgO/CaO mixed oxide exhibited the highest basicity, as it changed the colour of 4-nitroaniline (from brown to yellow) but not that of aniline (H_ = 27.0).

Based on the Hammett indicator results, the catalysts can thus be ranked in increasing order of basic strength as follows:

CaO < MgO = KNO_3/CaO 900 < KNO_3/CaO 700 < MgO/CaO.

3.2. Catalytic activity: Transesterification of glycerol with DEC

The reaction mechanism, **Error! Reference source not found.**, has been reported by different authors (21,29,54). It involves the exchange of a carbonyl group between an alcohol and a carbonate source, diethyl carbonate in this case. The first step of the heterogenous catalysis reaction mechanism involves proton abstraction by basic catalyst to form an intermediate glyceroxide anion. Then the latter attacks DEC as a nucleophile followed by the release of the first ethanol molecule. The new intermediate molecule undergoes an intramolecular nucleophilic substitution releasing the second ethanol molecule and forming GC as a final product.

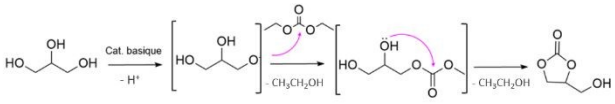

Figure 12: Mechanism of the transesterification reaction between Glycerol and DEC to form Glycerol Carbonate

The search for optimal conditions for the transcarbonatation reaction studied requires a special attention due to its endothermicity (ΔH° = 115.71 kJ/mol) and its non-spontaneous nature (ΔG° = 13.523 kJ/mol) (27,55). The reaction equilibrium can be shifted by using one of the reactants in excess and by removing the volatile product. Furthermore, a particular characteristic of the system arises from the non-miscibility of the reactants (27) and the variation of boiling point of the liquid medium during the reaction.

Two secondary reactions, oligomerisation and glycidol formation can occur according to transcarbonation conditions. Polycarbonate formation is undetectable by the usual analytical methods (FT-IR and GC FID). The formation of these oligomers results in a yellow/brown viscous product (19), as an indicator of the phenomenon. Oligomerisation is enhanced by the basicity of the catalyst promoting the opening of the GC ring formed (21). Oligomerization mechanisms lead to complex reactions depending on the involved group (ODO or hydroxyl). This mechanism is triggered when the reaction medium temperature exceeds 120-130 °C. Tests conducted at 130°C in the presence of a basic catalyst showed evidence of the oligomer formation, as discussed by some authors (21,23,56). On the other hand, the formation of glycidol, a highly reactive compound, is due to the deprotonation of primary alcohol group of GC by a strong base followed by an intermolecular nucleophilic substitution causing the GC ring opening. The closure of the epoxy ring is accompanied by the release of CO_2 molecule (57,58).

Several catalysts were tested for the transesterification reaction between glycerol and DEC. Glycerol conversion, glycerol carbonate yield and reaction selectivity were calculated for the different catalysts (**Error! Reference source not found.** and **Error! Reference source not found.**) based on the chromatograms (Figure 3 of ESI†). Generally, for this type of reaction, the catalyst efficiency requires a moderate base activity. The basic strength is necessary for the first step of the reaction (the abstraction of the primary hydroxyl group proton). In the heterogeneous medium, the catalytic reaction mainly occurs on the surface of the catalyst and the limiting factor is the reagents mass transport from the bulk solution to the catalyst's surface. The choice of CaO core was based on the results obtained for transcarbonation reaction using DMC and for transesterification leading to biodiesel (23,40,59–62).

In **Error! Reference source not found.**, the results obtained for the reactions with two earth metal carbonates showed high glycerol conversions. However, the selectivity of the reaction was limited due to the formation of carbonate oligomers observed as a brown deposit on the macroporous resin. It was found that after one hour of reaction, K_2CO_3 behaved more like a heterogeneous catalyst, due to the change in the medium composition. Since the separation of K_2CO_3 catalyst by centrifugation was incomplete. The use of a cationic exchange resin was necessary, as for the homogeneous Na_2CO_3 catalyst.

Table 4:Results obtained with homogeneous catalysts

Catalyst	% wt. / Gly	Glycerol Conversion (%)	GC Yield (%)	GC Selectivity (%)
Na_2CO_3	5	93 ± 4	58 ± 9	63 ± 12
	10	90 ± 4	54 ± 5	61 ± 3
K_2CO_3	5	90 ± 2	66 ± 11	74 ± 12
	10	89 ± 3	69 ± 9	77 ± 8

View Article Online
DOI: 10.1039/D5NJ03530A

ARTICLE

Table 5:Results obtained with heterogeneous catalysts

Catalyst	% wt. / Gly	Glycerol Conversion (%)	GC Yield (%)	GC Selectivity (%)
CaO	5	27 ± 1	2 ± 1	6 ± 1
	10	46 ± 1	1 ± 1	2 ± 1
MgO	5	41 ± 1	2 ± 1	6 ± 1
	10	43 ± 1	1 ± 1	2 ± 1
MgO/CaO	5	51 ± 2	49 ± 2	97 ± 4
	10	80 ± 4	74 ± 2	93 ± 3
KNO_3/CaO 700	5	92 ± 2	88 ± 2	96 ± 4
	10	93 ± 2	71 ± 2	76 ± 2
KNO_3/CaO 900	5	30 ± 1	2 ± 1	7 ± 1
	10	6 ± 1	4 ± 1	61 ± 1

Error! Reference source not found. displays the results obtained from experimental tests with the selected catalysts. It should be noted that the glycerol carbonate yields (and the resulting selectivities) in Table 5 do not take into account the glycerol carbonate trapped with the catalyst grains separated from the liquid phase by filtration. Calculations have shown that the yields of GC were underestimated by 5–16% for experiments involving the MgO/CaO and KNO_3/CaO 700 catalysts, meaning that the actual selectivities are higher than the reported values (Table 1 of ESI †.). The estimation was done by the mass balance carried out from the GC synthesis and its work-up. An example of the mass balance for KNO_3/CaO 700 5% wt/Gly catalyst is shown in Figure 4 of ESI †.

For the single metal heterogeneous oxides, CaO and MgO, we observe low GC yields. This result can be explained by the partial deactivation of CaO catalyst by interactions with H_2O and CO_2 (19). According to XRD analysis, the only phase present in CaO catalyst is the hexagonal $Ca(OH)_2$ hydrated phase. Moreover, the FTIR spectrum of the catalyst after reaction shows the presence of non-dissociated water on the catalyst's surface. Furthermore, the low basicity of CaO catalyst corroborates the average performance of these catalysts. For MgO, we could expect a lower basic strength, if we compare alkaline earth metals (group 2A – second column of the periodic table) with alkali metals (group 1A – first column of the periodic table). This assumption was confirmed by the low basicity of MgO catalytic sites ($9.3 < H_- < 15$).

The best catalytic performances were observed for mixed heterogeneous catalysts (MgO/CaO, 10% loading and KNO_3/CaO 700, 5% loading) with GC yields of 74% and 88% respectively. For MgO/CaO, when using the higher loading, a quantitative glycerol conversion and a good GC selectivity were obtained.

These results are in agreement with the previous works using mixed catalysts when DMC was employed as a carbonate source. Khayoon et al. (2013), reported a 100 % GC yield with MgO/CaO, at 70°C after 90 min (3). Likewise, Hu et al. (2025) obtained an 85 % GC yield (at 70°C after 2 h) with a catalyst based on KNO_3/CaO 700 catalyst (34).

In the case of mixed heterogeneous KNO_3/CaO 700 catalyst, we can observe that the lower catalyst loading provides a high GC selectivity, limiting the glycidol formation as a secondary product (no detected by GC). KNO_3/CaO 700 catalyst shows orthorhombic KNO_3 and cubic CaO structures according to XRD analysis (Figure 2 d)). Additionally, its high basic strength ($15 < H_- < 18.4$) can explain the catalytic activity as well as its crystallin structure.

The mixed KNO_3/CaO 900 catalyst displayed a very low catalytic activity at both loadings, probably due to the low measured basicity ($9.3 < H_- < 15$) and the particle agglomeration observed in the SEM images (Figure 10).

The results therefore confirm that coupling the active calcium core with another metal component as a support, can protect the active sites from air. Moreover, the association of the active CaO core with Mg^{2+} and K^+ led to a higher specific surface, while retaining mesoporous characteristics (average pore sizes in Table 3).

Finally, related homogeneous catalysts (alkali metals carbonates) showed a lack of selectivity for transcarbonation of glycerol with DEC. Furthermore, the use of homogeneous catalysts comes with

significant challenges in terms of separation and reusability, especially at larger scales. Heterogeneous base catalysis overcomes the limitations of homogeneous catalysis, and provides a more environmentally friendly alternative (63). It should be noted that studying the morphology of heterogeneous catalysts is necessary to understand the surface interactions between the reactants and the catalyst.

The selected mixed oxides can be easily separated from the final product and potentially reactivated to be reused.

4. Conclusion

This study highlights the feasibility of the transcarbonation reaction of glycerol with DEC in mild conditions and quantitative yields, thanks to two heterogeneous mixed metal oxide catalysts, MgO/CaO, (10%) and KNO_3/CaO 700 (5%). The results have demonstrated the advantages of using these easily prepared mixed oxides. These mixed oxides exhibit mesoporous characteristics and high basic basicity ($H_- > 15$) making them suitable for the transcarbonation reaction. The superior performance of KNO_3/CaO calcinated at 700 °C can be attributed to its stability in air and its crystalline form.

The different analyses confirmed that the calcination temperature played a significant role in catalytic activity, as it influences the crystal lattice structure and the morphology of particles. We identified a minimum calcination temperature (650 °C for the studied oxides) and a critical calcination temperature to be considered.

The results of this work open up new perspectives and demonstrate strong potential for the development of a glycerol transcarbonation process using DEC as a carbonate source, made possible by the use of heterogeneous catalysts based on mixed metal oxides. These catalysts, easy to prepare and efficient under mild conditions, promote the development of novel production processes that optimize yields while minimizing environmental impact. In the future, the integration of process intensification strategies such as reactive distillation, membrane reactors or advanced heating technologies could significantly enhance productivity, selectivity, and energy efficiency. These approaches offer a promising path toward the industrial scale-up of an environmentally friendly process in line with principles of green chemistry and sustainable development.

Data availability

The data supporting this article have been included as part of ESI.†

Author contributions

Linda Miturova: Conceptualisation, Data curation, Methodology, Formal Analysis, Investigation, Visualisation, Writing – original draft

Ivonne Rodriguez-Donis: Conceptualisation, Funding Acquisition, Methodology, Supervision, Validation, Writing – review and editing

Pascale De Caro: Conceptualisation, Funding Acquisition, Methodology, Supervision, Validation, Writing – review and editing

Conflicts of interest

There are no conflicts to declare

Acknowledgements

This work was supported by the French state through the National Research Agency under the Program for Future Investments bearing the reference ANR-18-EURE-0021.
The financial support was provided by the network Carnot 3BCAR (GreenCarGly program) and the French Ministry of Higher Education and Research (MESR).

References

1. Ambat I, Srivastava V, Sillanpää M. Recent advancement in biodiesel production methodologies using various feedstock: A review. Renewable and Sustainable Energy Reviews. 2018 July 1;90:356–69.

2. Kibar ME, Hilal L, Çapa BT, Bahçıvanlar B, Abdeljelil BB. Assessment of Homogeneous and Heterogeneous Catalysts in Transesterification Reaction: A Mini Review. ChemBioEng Reviews. 2023;10(4):412–22.

3. Khayoon MS, Hameed BH. Mg1+xCa1−xO2 as reusable and efficient heterogeneous catalyst for the synthesis of glycerol carbonate via the transesterification of glycerol with dimethyl carbonate. Applied Catalysis A: General. 2013 Sept 10;466:272–81.

4. Sonnati MO, Amigoni S, Givenchy EPT de, Darmanin T, Choulet O, Guittard F. Glycerol carbonate as a versatile building block for tomorrow: synthesis, reactivity, properties and applications. Green Chem. 2013 Jan 28;15(2):283–306.

5. de Caro P, Bandres M, Urrutigoïty M, Cecutti C, Thiebaud-Roux S. Recent Progress in Synthesis of Glycerol Carbonate and Evaluation of Its Plasticizing Properties. Front Chem. 2019 May 24;7.

6. Salari M, Varela JC, Zhang H, Grinstaff MW. Sustainable glycerol carbonate electrolytes for Li-ion supercapacitors: performance evaluation of butyl, benzyl, and ethyl glycerol carbonates. Mater Adv. 2021;2(18):6049–57.

7. Prete P, Trano S, Zaccagnini P, Fagiolari L, Amici J, Lamberti A, et al. Glycerol carbonate and solketal carbonate as circular economy bricks for supercapacitors and potassium batteries. ChemSusChem. n/a(n/a):e202401636.

8. Rozulan N, Halim SA, Razali N, Lam SS. A review on direct carboxylation of glycerol waste to glycerol carbonate and its applications. Biomass Conv Bioref. 2022 Oct 1;12(10):4665–82.

9. Valentin R, Alignan M, Giacinti G, Renaud FNR, Raymond B, Mouloungui Z. Pure short-chain glycerol fatty acid esters and glycerylic cyclocarbonic fatty acid esters as surface active and antimicrobial coagels protecting surfaces by promoting superhydrophilicity. Journal of Colloid and Interface Science. 2012 Jan 1;365(1):280–8.

10. Holmiere S, Valentin R, Maréchal P, Mouloungui Z. Esters of oligo-(glycerol carbonate-glycerol): New biobased oligomeric surfactants. Journal of Colloid and Interface Science. 2017 Feb;487:418–25.

11. Nohra B, Candy L, Blanco JF, Guerin C, Raoul Y, Mouloungui Z. From Petrochemical Polyurethanes to Biobased Polyhydroxyurethanes. Macromolecules. 2013 May 28;46(10):3771–92.

12. Fitzgerald DM, Zhang H, Bordeianu C, Colson YL, Grinstaff MW. Synthesis of Polyethylene Glycol–Poly(glycerol carbonate) Block Copolymeric Micelles as Surfactant-Free Drug Delivery Systems. ACS Macro Lett. 2023 July 18;12(7):974–9.

13. Franklin S. Carbonate-haloformate of glycerol and method of producing same [Internet]. 2446145, 1948. Available from: https://www.freepatentsonline.com/2446145.html

14. Behr A, Eilting J, Irawadi K, Leschinski J, Lindner F. Improved utilisation of renewable resources: New important derivatives of glycerol. Green Chemistry. 2008;10(1):13–30.

15. Nomanbhay S, Ong MY, Chew KW, Show PL, Lam MK, Chen WH. Organic Carbonate Production Utilizing Crude Glycerol Derived as By-Product of Biodiesel Production: A Review. Energies. 2020 Jan;13(6):1483.

16. Yadav GD, Chandan PA. A green process for glycerol valorization to glycerol carbonate over heterogeneous hydrotalcite catalyst. Catalysis Today. 2014 Nov 15;237:47–53.

17. Claude S, Mouloungui Z, Yoo JW, Gaset A. Procédé de fabrication de carbonate de glycérol. EP0955298A1, 1999. Available from: https://patents.google.com/patent/EP0955298A1/fr

18. van Dam RA, Hogan AC, McCullough CD, Houston MA, Humphrey CL, Harford AJ. Aquatic toxicity of magnesium sulfate, and the influence of calcium, in very low ionic concentration water. Environmental Toxicology and Chemistry. 2010;29(2):410–21.

19. Ochoa-Gómez JR, Gómez-Jiménez-Aberasturi O, Maestro-Madurga B, Pesquera-Rodríguez A, Ramírez-López C, Lorenzo-Ibarreta L, et al. Synthesis of glycerol carbonate from glycerol and dimethyl carbonate by transesterification: Catalyst screening and reaction optimization. Applied Catalysis A: General. 2009 Sept;366(2):315–24.

20. Okoye PU, Abdullah AZ, Hameed BH. Glycerol carbonate synthesis from glycerol and dimethyl carbonate using trisodium phosphate. Journal of the Taiwan Institute of Chemical Engineers. 2016 Nov;68:51–8.

21. Rokicki G, Rakoczy P, Parzuchowski P, Sobiecki M. Hyperbranched aliphatic polyethers obtained from environmentally benign monomer: glycerol carbonate. Green Chem. 2005;7(7):529.

22. Pradhan G, Sharma YC. Green synthesis of glycerol carbonate by transesterification of bio glycerol with dimethyl carbonate over Mg/ZnO: A highly efficient heterogeneous catalyst. Fuel. 2021 Jan 15;284:118966.

23. Praikaew W, Kiatkittipong W, Aiouache F, Najdanovic-Visak V, Ngaosuwan K, Wongsawaeng D, et al. Process and Energy Intensification of Glycerol Carbonate Production from Glycerol and Dimethyl Carbonate in the Presence of Eggshell-Derived CaO Heterogeneous Catalyst. Energies. 2021 Jan;14(14):4249.

24. Pacheco MA, Marshall CL. Review of Dimethyl Carbonate (DMC) Manufacture and Its Characteristics as a Fuel Additive. Energy Fuels. 1997 Jan 1;11(1):2–29.

25. Patraşcu I, Bîldea CS, Kiss AA. Novel eco-efficient reactive distillation process for dimethyl carbonate production by indirect alcoholysis of urea. Front Chem Sci Eng. 2022 Feb 1;16(2):316–31.

26. Zhang Z, Xu H, Zhang Q, Zhang A, Li Y, Li W. Separation of methanol + dimethyl carbonate azeotropic mixture using ionic liquids as entrainers. Fluid Phase Equilibria. 2017 Mar 15;435:98–103.

27. Liu J, Pan D, Zhang Q, Guan Y, Yang B. Liquid-liquid equilibrium of immiscible systems involved in glycerol transesterification with diethyl carbonate. Fluid Phase Equilibria. 2022 July;558:113455.

28. Tundo P, Aricò F, Rosamilia AE, Rigo M, Maranzana A, Tonachini G. Reaction of dialkyl carbonates with alcohols: Defining a scale of the best leaving and entering groups. Pure and Applied Chemistry. 2009 Oct 31;81(11):1971–9.

29. Alvarez MG, Segarra AM, Contreras S, Sueiras JE, Medina F, Figueras F. Enhanced use of renewable resources: Transesterification of glycerol catalyzed by hydrotalcite-like compounds. Chemical Engineering Journal. 2010 July 15;161(3):340–5.

30. Álvarez MG, Plíšková M, Segarra AM, Medina F, Figueras F. Synthesis of glycerol carbonates by transesterification of glycerol in a continuous system using supported hydrotalcites as catalysts. Applied Catalysis B: Environmental. 2012 Feb;113–114:212–20.

31. Souza Júnior RL, Rossi TM, Detoni C, Souza MMVM. Glycerol carbonate production from transesterification of glycerol with diethyl carbonate catalyzed by Ca/Al-mixed oxides derived from hydrocalumite. Biomass Conv Bioref. 2023 Jan 1;13(2):661–73.

32. Wu Y, Song X, Cai F, Xiao G. Synthesis of glycerol carbonate from glycerol and diethyl carbonate over Ce-NiO catalyst: The

role of multiphase Ni. Journal of Alloys and Compounds. 2017 Oct 5;720:360–8.

33. Andola SC, Pandey A, Kothari AC, Singh G, Singh A, Malik R. Green Synthesis of Glycerol Carbonate from Glycerol Over Prepared Sodium Aluminate Catalysts by Spray Drying. Catal Lett. 2025 July 1;155(7):1–15.

34. Hu K, Wang H, Liu Y, Yang C. KNO3/CaO as cost-effective heterogeneous catalyst for the synthesis of glycerol carbonate from glycerol and dimethyl carbonate. Journal of Industrial and Engineering Chemistry. 2015 Aug 25;28:334–43.

35. Koranian P, Dalai AK, Sammynaiken R. Structural study of mixed metal oxide catalysts comprising Mg, Ca, and Al used for upgrading biodiesel byproduct glycerol to glycerol carbonate. Applied Catalysis A: General. 2024 June 2;679:119727.

36. Freeman ES. The Kinetics of the Thermal Decomposition of Potassium Nitrate and of the Reaction between Potassium Nitrite and Oxygen1a. J Am Chem Soc. 1957 Feb 1;79(4):838–42.

37. Kramer CM, Munir ZA, Volponi JV. Screening tests of sodium nitrate and potassium nitrate decomposition. Solar Energy. 1982 Jan 1;29(5):437–9.

38. R. Nelson J, J. Needs R, J. Pickard C. Calcium peroxide from ambient to high pressures. Physical Chemistry Chemical Physics. 2015;17(10):6889–95.

39. Arora S, Gosu V, Kumar UKA, Zhang TC, Subbaramaiah V. A novel Ce-CaO/MgO catalyst derived from marble waste through green synthesis route for glycerol carbonate synthesis. Reac Kinet Mech Cat. 2021 Apr 1;132(2):839–58.

40. Kaur A, Ali A. Surface-Modified CaO Catalyst for the Production of Glycerol Carbonate. ChemistrySelect. 2021;6(24):6102–14.

41. Barker R. The reactivity of calcium oxide towards carbon dioxide and its use for energy storage. Journal of Applied Chemistry and Biotechnology. 1974;24(4–5):221–7.

42. Glasson DR. Reactivity of lime and related oxides. I. Production of calcium oxide. Journal of Applied Chemistry. 1958;8(12):793–7.

43. Sun YH, Sun LB, Li TT, Liu XQ. Modulating the Host Nature by Coating Alumina: A Strategy to Promote Potassium Nitrate Decomposition and Superbasicity Generation on Mesoporous Silica SBA-15. J Phys Chem C. 2010 Nov 11;114(44):18988–95.

44. Algoufi YT, Kabir G, Hameed BH. Synthesis of glycerol carbonate from biodiesel by-product glycerol over calcined dolomite. Journal of the Taiwan Institute of Chemical Engineers. 2017 Jan 1;70:179–87.

45. Alonso DM, Mariscal R, Moreno-Tost R, Poves MDZ, Granados ML. Potassium leaching during triglyceride transesterification using K/γ-Al2O3 catalysts. Catalysis Communications. 2007 Dec 1;8(12):2074–80.

46. Wang Y, Chen Y, Liu C, Yu F, Chi Y, Hu C. The effect of magnesium oxide morphology on adsorption of Cr(VI) from aqueous solution. Chemical Engineering Journal. 2017 May 15;316:936–50.

47. Olutoye MA, Lee SC, Hameed BH. Synthesis of fatty acid methyl ester from palm oil (Elaeis guineensis) with Ky(MgCa)2xO3 as heterogeneous catalyst. Bioresource Technology. 2011 Dec 1;102(23):10777–83.

48. Chen Q, Hui T, Sun H, Peng T, Ding W. Synthesis of magnesium carbonate hydrate from natural talc. Open Chemistry. 2020 Jan 1;18(1):951–61.

49. Zhou J, Yang S, Yu J. Facile fabrication of mesoporous MgO microspheres and their enhanced adsorption performance for phosphate from aqueous solutions. Colloids and Surfaces A: Physicochemical and Engineering Aspects. 2011 Apr 20;379(1):102–8.

50. Taufiq-Yap YH, Lee HV, Yunus R, Juan JC. Transesterification of non-edible *Jatropha curcas* oil to biodiesel using binary Ca–Mg mixed oxide catalyst: Effect of stoichiometric composition. Chemical Engineering Journal. 2011 Dec 15;178:342–7.

51. Manual of Symbols and Terminology for Physicochemical Quantities and Units, Appendix II: Definitions, Terminology and Symbols in Colloid and Surface Chemistry. Pure and Applied Chemistry. 1976 Jan 1;46(1):71–90.

52. Catalin I, Verdes O, Suba M. Nitrogen Sorption Measurements and Thermal Analysis Techniques. In: Microbial Electrochemical Technologies. John Wiley & Sons, Ltd; 2023. p. 229–44. Available from: https://onlinelibrary.wiley.com/doi/abs/10.1002/9783527839001.ch8

53. Taiswa A, Maglinao RL, Andriolo JM, Kumar S, Skinner JL. Electrospun Pt-TiO2 nanofibers Doped with HPA for Catalytic Hydrodeoxygenation. Sci Rep. 2024 Oct 21;14(1):24706.

54. Ji Y. Recent Development of Heterogeneous Catalysis in the Transesterification of Glycerol to Glycerol Carbonate. Catalysts. 2019 July;9(7):581.

55. Zhang J, Wu Y, Song X, Xu S, Li S, Zhu Y, et al. Thermodynamic and kinetic studies for synthesis of glycerol carbonate from glycerol and diethyl carbonate over Ce–NiO catalyst. Chem Pap. 2018 Nov 1;72(11):2909–19.

56. Pradhan G. Green synthesis of glycerol carbonate by transesterification of bio glycerol with dimethyl carbonate over Mg/ZnO_ A highly efficient heterogeneous catalyst. 2021;

57. Ochoa-Gómez JR, Gómez-Jiménez-Aberasturi O, Ramírez-López C, Maestro-Madurga B. Synthesis of glycerol 1,2-carbonate by transesterification of glycerol with dimethyl carbonate using triethylamine as a facile separable homogeneous catalyst. Green Chem. 2012;14(12):3368.

View Article Online
DOI: 10.1039/D5NJ03530A

58. Darensbourg DJ, Yeung AD. Kinetics and thermodynamics of the decarboxylation of 1,2-glycerol carbonate to produce glycidol: computational insights. Green Chem. 2014;16(1):247–52.

59. Bazargan A, Kostić MD, Stamenković OS, Veljković VB, McKay G. A calcium oxide-based catalyst derived from palm kernel shell gasification residues for biodiesel production. Fuel. 2015 June 15;150:519–25.

60. Simanjuntak FSH, Kim TK, Lee SD, Ahn BS, Kim HS, Lee H. CaO-catalyzed synthesis of glycerol carbonate from glycerol and dimethyl carbonate: Isolation and characterization of an active Ca species. Applied Catalysis A: General. 2011 July 15;401(1):220–5.

61. Laca A, Laca A, Díaz M. Eggshell waste as catalyst: A review. Journal of Environmental Management. 2017 July 15;197:351–9.

62. Boey PL, Maniam GP, Hamid SA. Performance of calcium oxide as a heterogeneous catalyst in biodiesel production: A review. Chemical Engineering Journal. 2011 Mar 15;168(1):15–22.

63. Kaur N, Banik N. Industrial Applications of Solid Base Catalysis. In: Solid Base Catalysts. John Wiley & Sons, Ltd; 2024. p. 169–231.Available from: https://onlinelibrary.wiley.com/doi/abs/10.1002/9783527846719.ch7

View Article Online
DOI: 10.1039/D5NJ03530A

Data availability Statement

The data supporting this article have been included as part of the Supplementary Information.